Accepted Manuscript

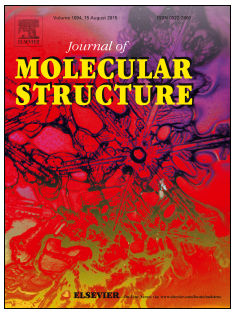

Novel triazole and morpholine substituted bisnaphthalimide: Synthesis, photophysical and G-quadruplex binding properties

Zhize Ou, Zhiyuan Li, Yunyan Gao, Wenli Xing, Hongdan Jia, Huan Zhang, Na Yi

PII: S0022-2860(19)30203-0

DOI: https://doi.org/10.1016/j.molstruc.2019.02.073

Reference: MOLSTR 26230

To appear in: *Journal of Molecular Structure*

Received Date: 11 December 2018

Revised Date: 5 February 2019

Accepted Date: 19 February 2019

Please cite this article as: Z. Ou, Z. Li, Y. Gao, W. Xing, H. Jia, H. Zhang, N. Yi, Novel triazole and morpholine substituted bisnaphthalimide: Synthesis, photophysical and G-quadruplex binding properties, *Journal of Molecular Structure* (2019), doi: https://doi.org/10.1016/j.molstruc.2019.02.073.

Graphic abstract

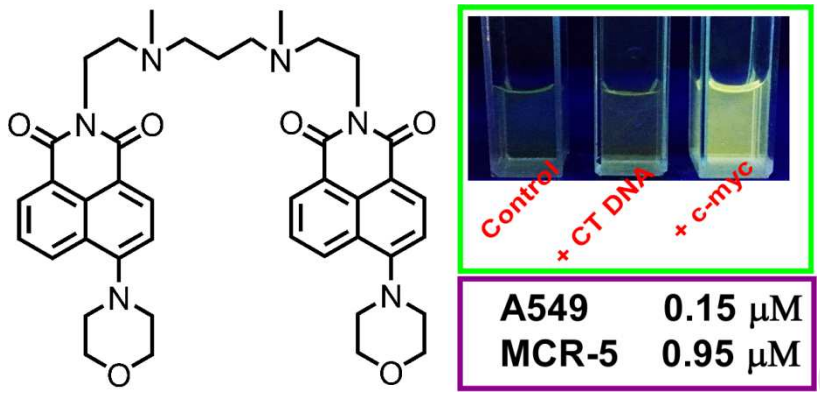

The bisnaphthalimide, with high affinity toward G-quadruplex DNA, is able to inhibit the growth of lung cancer A549 cells selectively over non-cancerous MRC-5 cells.

Department of Applied Chemistry,
School of Science,
Northwestern Polytechnic University,
Xi'an 710072, P. R. China
E-mail: gaoyunyan@nwpu.edu.cn

Dear Editor:

Thank you for your e-mail and for the reviewers' comments concerning our manuscript entitled "Novel triazole and morpholine substituted bisnaphthalimide: synthesis, photophysical and G-quadruplex binding properties" (Manuscript ID: MOLSTRUC-D-18-03754). We have carried out some experiments and revised the manuscript according to reviewers' comments, with the revised parts marked in red. We hope that could meet with their approval.

We would like to express our appreciation to you and to the reviewers for suggesting how to improve our paper. We also responded point by point to the referee's comments as listed below, along with a clear indication of the location of the revision in the manuscript.

Thank you.

Sincerely Yours,
Yunyan Gao
Professor of Chemistry

Novel triazole and morpholine substituted bisnaphthalimide: synthesis, photophysical and G-quadruplex binding properties

Zhize Ou, Zhiyuan Li, Yunyan Gao*, Wenli Xing, Hongdan Jia, Huan Zhang, Na Yi

The Key Laboratory of Space Applied Physics and Chemistry, Ministry of Education, Department of Applied Chemistry, School of Science, Northwestern Polytechnical University, Xi'an 710072, P. R. China.

Corresponding Author:

Yunyan Gao

Department of Applied Chemistry, School of Science

Northwestern Polytechnical University

Xi'an 710072

P. R. China

E-mail: gaoyunyan@nwpu.edu.cn

Abstract

Four bisnaphthalimides derivatives **3a**, **3b**, **5a** and **5b** with polyamine linkage have been synthesized and characterized. Different spectroscopic techniques, including UV-Vis spectroscopy, fluorescence spectroscopy, circular dichroism and fluorescence resonance energy transfer (FRET), have been used to explore the interaction of these compounds with G-quadruplex structures (Htelo, c-myc, c-kit). The compounds **3a**, **3b** and **5b** show high affinity toward Htelo, c-myc and c-kit G-quadruplexes ($K_a > 4.42\times10^6$ M^{-1}), and exhibit more than 40-fold selectivity for the quadruplex versus CT DNA. Binding of **3a**, **3b** to telomeric and oncogenic G-quadruplexes induce strong enhancement of the fluorescence intensity (18 to 27-fold), whereas the duplex CT DNA induces much weaker fluorescence enhancement (around 2-fold). Being fluorescent, the cellular localization of **3a**, **3b** can be conveniently tracked by fluorescence imaging. The results indicate that **3a**, **3b** can readily be taken up by A549 lung cancer cells. Molecular docking studies indicate that **3a**, **3b**, **5a** and **5b** mainly bind in the groove and/or loop region of the G-quadruplexes, and hydrogen bonding plays an important role in the interaction of bisnaphthalimide derivatives with G-quadruplexes. CD spectroscopy and FRET melting assay indicate that **3a**, **3b** and **5b** can promote the formation and the stabilization of human telomeric and c-myc G-quadruplex DNA. The compound **3b** can inhibit the growth of A549 cells (IC_{50} = 0.15 μM), with a much higher antitumor activity than amonafide.

Keywords: G-quadruplex; bisnaphthalimide; anticancer drug; AutoDock; fluorescence probe

1. Introduction

The Guanine-rich nucleic acid sequences are prevalent in human genes, especially in telomere ends and promoters of some functionally important proto-oncogenes [1-3]. The guanine tracts in these sequences can fold into G-quadruplexes (G4) via Hoogsten hydrogen bonds. There are evidences that G4s are involved in a variety of biological processes [4,5]. Human telomeric DNA consists of tandem repeats of the sequence 5'-d(TTAGGG)-3', which protects chromosomes from degradation and is essential for ensuring genomic stability. The telomerase is selectively expressed in the majority of human cancer cells, and its activation is thought to be a critical step in cellular immortalization and tumorigenesis. The telomeric G4 stabilizing ligands can inhibit telomerase activity and induce growth arrest in cancer cells [6]. On the other hand, the proto-oncogenes play critical roles in the regulation of programmed cell death or apoptosis. The abnormal overexpress of the proto-oncogenes has recently been shown in tumors. For example, the c-myc proto-oncogene, overexpressed in up to 80% of solid tumors, such as gastrointestinal, ovarian and breast cancer tumors [7,8]. The proto-oncogenes can be transcriptionally repressed by targeting a putative G4 with small molecules [9,10]. A large number of small molecules and metal complexes, such as phorphyrin derivatives, carbazole derivatives, quindolines, peptide and quarflxoxin can bind G4s and modulate the gene expression [11-16]. Thus, G4s are considered as a promising new class of targets for the design of anticancer drugs [17-20].

Naphthalimide derivatives, as a class of DNA-binding agents, have been extensively explored as antitumor agents [21]. However, naphthalimide-based anti-tumor drugs may cause serious side effects, including central neurotoxicity and dose-limiting toxicity. In order to improve their potency and reduce the side effects, naphthalimide derivatives, modified with fused aromatic rings,

side chains and imide substituents have been synthesized [22-26]. Recently, the studies of the sequence-specific binding of naphthalimides to DNA have been an important topic in the design of novel drugs [27]. The trisubstituted naphthalimide derivatives can bind telomeric G-quadruplexes with high affinity and show antiproliferation activity against various cell lines [28]. We have also synthesized a series of naphthalimides modified with thiourea, imidazole and terpyridine complexes, which possess high affinity ($K_a > 10^6\ M^{-1}$) and reasonable selectivity for telomeric G-quadruplex DNA over duplex DNA [29-31].

It has been reported that the bisnaphthalimides bisnafide and elinafide present potent cellular cytotoxicity and excellent in vivo antitumor activity, and have been selected for clinical trials [32]. The substituents at naphthalimide skeleton and linkers play crucial roles in determining the sequence selectivity, photophysical properties and cytotoxic activity of bisnaphthalimides derivatives [33-38]. However, to the best of our knowledge, there is no report about the interaction between bisnaphthalimide and G-quadruplexes. In this study, the bisnaphthalimides with alkyl amino linkages are synthesized. The flexible polyamine-bridge can facilitate the electrostatic interactions with the loops and grooves of the phosphate backbone of G4 DNA [39]. The morpholine and 1,2,3-triazole moieties are incorporated at the 4-position of the bisnaphthalene ring to enhance their G4 binding ability and cytotoxic activity [40,41]. The association of bisnaphthalimides with telomeric and oncogenic promoter G4s, including c-myc and c-kit quadruplex, is investigated in detail by spectroscopic techniques and molecular docking studies. Systematic investigation of the interaction between bisnaphthalimde and G4s can provide structural insight into recognition of G-quadruplex by naphthalimides, and can be helpful for the design of G-quadruplex targeting agents.

2 Experimental

2.1 Materials

1-(4,5-Dimethyl-2-thiazolyl)-3,5-diphenylformazan (MTT), 4,6-diamino-2-phenylindole (DAPI), calf thymus DNA (CT DNA) and 4-bromo-1,8-naphthalic anhydride were purchased from Sigma-Aldrich. The Htelo strand (5'-GGG-TTA-GGG-TTA-GGG-TTA-GGG-3') was used for the human telomeric studies. The oligomer strand (5'-TTG-AGG-GTG-GGT-AGG-GTG-GGT-AA-3') and (5'-AGG-GAG-GGC-GCT-GGG-AGG-AGGG-3') were used for c-myc and c-kit G4 studies, respectively. All DNA oligomers were purchased from Sangon (Shanghai, China) and purified by Waters 2695 Alliance HPLC (U.S.A). Other chemicals of analytical grade were obtained from Beijing Chemical Plant. The organic solvents were distilled prior to use.

Unless otherwise stated, spectroscopic titration experiments were performed in HEPES buffer (10 mM, pH 7.4). Stocking solutions of bisnaphthalimides (1 mM) were prepared in dimethyl sulfoxide (DMSO).

2.2. Instrumentation

^{1}H NMR spectra were measured on a Bruker Avance 400 spectrometer. ^{13}C NMR spectra were measured on a Bruker Avance 600 spectrometer. Chemical shifts were given in parts per million (TMS as internal standard). Steady state absorption and fluorescence spectra were recorded using a Hitachi UV-3010 UV-Vis spectrophotometer and a Hitachi F-4600 spectrofluorimeter, respectively. For quantum yield calibration, 9,10-diphenylanthralene in ethanol was measured under the same excitation and detection conditions (fluorescence quantum yield of 9,10-diphenylanthralene in ethanol is 0.95) [42].

2.3 Synthesis

2.3.1 4-morpholine-1-yl- 1,8-naphthalic anhydride (2)

The morpholine (0.94 mL, 10.8 mmol) was added to a suspension of 4-bromo-1,8-naphthalic anhydride **1** (1.5 g, 5.4 mmol) in ethylene glycol (10 mL). The mixture was heated to reflux for 24 h under N_2 atmosphere. The solvent was removed under vacuum. Then the residue was purified by column chromatography on silica gel eluting with THF/$CHCl_3$ (1/4, v/v) to give 1.33 g yellow solid (yield, 86%). ^{1}H NMR ($CDCl_3$, 400 MHz) δ: 8.60 (d, 1H, *J* = 7.2 Hz), 8.54–8.48 (m, 2H), 7.78–7.75 (m, 1H), 7.29–7.26 (m, 1H), 4.07–4.05 (m, 4H), 3.36–3.33 (m, 4H).

2.3.2 *N,N'*-Bis[2-((4-morphine-1-yl)-naphthalimide)ethyl]propane-1,3-diamine (3a)

To a hot suspension of compound **2** (0.5 g, 1.75 mmol) and triethylamine (0.5 mL) in 1,4-dioxiane (5 mL), *N,N*-bis(2-aminoethyl)propane-1,3-diamine (140 mg, 0.875 mmol) was added dropwise. The reaction mixture was refluxed for 48 h in dark. The solvent was removed under vacuum. The residue was purified by column chromatography on silica gel eluting with $CH_3OH/CHCl_3$ (1/9, v/v). The yellow solid was obtained of 0.445 g, yield of 63.3%. ^{1}H NMR ($CDCl_3$, 400 MHz) δ: 8.57 (d, 2H, *J* = 7.2 Hz), 8.54 (d, 2H, *J* = 8.0 Hz), 8.42 (d, 2H, *J* = 8.4 Hz), 7.72 (m, 2H), 7.23 (d, 2H, *J* = 8.0 Hz), 4.28 (m, 4H), 4.02 (m, 8H), 3.25 (m, 8H), 2.960 (m, 4H), 2.757 (m, 4H), 1.86 (s, 2H), 1.69 (m, 2H). ^{13}C NMR ($CDCl_3$, 150 MHz) (ppm): 164.5, 164.0, 155.5, 132.5, 131.2, 130.0, 129.9, 126.1, 125.8, 123.2, 117.1, 114.9, 66.9, 53.4, 47.9, 47.7, 39.7, 30.0. MS (MAIDI-TOF): $[M]^+$ 691.6, calcd for $C_{39}H_{42}N_6O_6$, 690.8.

2.3.3 *N,N'*-Bis[2-((4-morphine-1-yl)-naphthalimide)ethyl]-N,N'-dimethylpropane -1,3-diamine (3b)

The compound **3a** (100 mg, 0.145 mmol) was suspended in 10 mL of ice-cold methanol,

followed by the addition of glacial acetic acid (0.126 g, 2.10 mmol), sodium cyanoborohydride (62.9 mg, 1.0 mmol), and left stirring in the ice bath for 20 min. An aqueous solution of 39% (v/v) formaldehyde (0.11 mL, 1.43 mmol) in 3 mL of methanol was added dropwise to the reaction mixture over a period of 30 min. The ice bath was removed and the reaction mixture was stirred at room temperature for 5 h. To adjust the pH, 25 mL of Na_2CO_3 solution (2%) was added, and the mixture was extracted with chloroform three times (3×20 mL). The extract was washed with a saturated solution of NaCl, dried over $MgSO_4$, concentrated under vacuum. The solid obtained was purified by column chromatography ($CH_3OH/CHCl_3$ =1/25, v/v). The yellow solid was obtained of 70 mg, yield of 42.6%. ^{1}H NMR ($CDCl_3$, 400 MHz) δ: 8.58 (d, 2H, *J* = 7.2 Hz), 8.52 (d, 2H, *J* = 8.0 Hz), 8.41 (d, 2H, *J* = 8.4 Hz), 7.69 (m, 2H), 7.23 (d, 2H, *J* = 8.0 Hz), 4.26 (m, 4H), 4.02 (m, 8H), 3.25 (m, 8H), 2.67 (m, 4H), 2.47 (m, 4H), 2.33 (s, 6H), 1.66 (s, 2H). ^{13}C NMR ($CDCl_3$, 150 MHz) (ppm): 164.3, 163.8, 155.5, 132.4, 131.1, 129.9, 129.8, 126.1, 125.8, 123.3, 117.2, 114.9, 66.9, 55.7, 54.6, 53.4, 42.3, 37.6, 29.7, 25.1. MS (MAIDI-TOF): $[M]^+$ 719.7, calcd for $C_{41}H_{46}N_6O_6$, 718.8.

2.3.4 4-(4-Phenyl-[1,2,3]-triazol-1-yl)-1,8-naphthalic anhydride (**4**)

The compound **4** was prepared according to the literature with slight modification [43]. To a suspension of 4-bromo-1,8-naphthalic anhydride **1** (1.0 g, 3.61 mmol) in 30 mL N-Methyl pyrrolidone (NMP) was added a solution of sodium azide (0.70 g, 10.8 mmol) in water (3 mL). The mixture was stirred vigorously for 5 h at 60 ℃, and the solution was poured into ice water. The precipitated yellow solid was filtered to give 4-azido-1,8-naphthalic anhydride.

The crude product 4-azido-1,8-naphthalic anhydride and ethynylbenzene (0.37 g, 3.61 mmol)

were suspended in DMF (10 mL). To this solution, copper(II) sulfate pentahydrate (21.0 mg, 0.08 mmol) was added, followed by sodium ascorbate (33 mg, 0.17 mmol). The mixture was heated at 60 °C for 14 h and poured into ice water. The product was collected by filtration. After washing the precipitate with cold water and methanol, the desired product was obtained (0.98 g, 80 % yield) as a yellow powder. ^{1}H NMR (DMSO-d_6, 400 MHz, ppm): 9.38 (s, 1H), 8.73–8.67 (m, 2H), 8.46–8.44 (m, 1H), 8.24 (d, 1H, J = 8 Hz), 8.06–8.02 (m, 3H), 7.58–7.54 (m, 2H), 7.46–7.43 (m, 1H).

2.3.5 *N,N'*-Bis[2-(4-(4-Phenyl-[1,2,3]-triazol-1-yl)-naphthalimide)ethyl]propane- 1,3-diamine (5a)

The procedure was similar to that of compound **3a**, except that the compound **4** was used in place of compound **2**. Yield: 52.8%. ^{1}H NMR (DMSO-d_6, 400 MHz) (ppm) δ: 9.30 (s, 2H), 8.64–8.59 (m, 4H), 8.34–8.29 (m, 2H), 8.15 (d, 2H, J = 8.0 Hz), 8.03–8.01 (d, 4H, J = 8.0 Hz), 7.97–7.93 (m, 2H), 7.55–7.52 (m, 4H), 7.44–7.41 (m, 2H), 4.19–4.16 (m, 4H), 2.88–2.85 (m, 4H), 2.70–2.67 (m, 4H), 1.60–1.56 (m, 2H). ^{13}C NMR (DMSO-d_6, 600 MHz) (ppm) δ: 163.30, 162.77, 147.05, 137.53, 131.50, 130.38, 129.92, 129.04, 129.01, 128.81, 128.41, 128.35, 125.64, 125.50, 124.05, 124.02, 123.41, 122.61, 47.00, 46.39, 45.67, 28.42. MS (ESI-MS): calcd for $C_{47}H_{38}N_{10}O_4$, 806.87.

2.3.6 *N,N'*-Bis[2-(4-(4-Phenyl-[1,2,3]-triazol-1-yl)-naphthalimide)ethyl]-N,N'-dimethylpropane-1,3-diamine (5b)

The procedure was similar to that of compound **3b**, except that the compound **5a** was used in place of compound **3a**. Yield: 53.0%. ^{1}H NMR (DMSO-d_6, 400 MHz) δ: 9.22 (s, 2H), 8.59–8.53 (m, 4H), 8.24 (d, 2H, J = 8.0 Hz), 8.09 (d, 2H, J = 8.0 Hz), 7.99 (d, 4H, J = 8.0 Hz), 7.89–7.85 (m, 2H), 7.53–7.50 (m, 4H), 7.43–7.39 (m, 2H), 4.07–4.03 (m, 4H), 2.48–2.45 (m, 4H), 2.35–2.26 (m,

4H), 2.15 (s, 6H), 1.46 (s, 2H) . ^{13}C NMR (DMSO-d_6, 600 MHz) (ppm) δ: 163.02, 162.49, 146.99, 137.54, 131.53, 130.44, 129.90, 129.43, 128.99, 128.76, 128.40, 128.30, 125.58, 125.50, 123.96, 123.92, 123.21, 122.44, 54.85, 53.89, 42.13, 37.47, 18.53. MS (ESI-MS): 835.1M^+, calcd for $C_{49}H_{42}N_{10}O_4$, 834.92.

2.4 Determination of lipophilicity (logP)

To obtain octanol-saturated water (OSW) and water-saturated octanol (WSO), 100 mL of water was stirred with 100 mL of octanol for 24 h, followed by centrifugation for 5 min. The bisnaphthalimides were dissolved in 5.0 mL of OSW to a typical concentration of 0.05 mM and then mixed with 5.0 mL WSO. The samples were mixed, stirred for 24 h at room temperature and then centrifuged for 5 min. The layers were separated carefully, and the concentrations of bisnaphthalimides in WSO and OSW were determined by UV-Vis spectroscopy. Partition coefficients of bisnaphthalimides were calculated using the equation (eqn (1)):

$$\log P = \log ([\text{compound}]_{WSO}/[\text{compound}]_{OSW}) \quad (1)$$

where $[\text{compound}]_{WSO}$ and $[\text{compound}]_{OSW}$ was the concentration of bisnaphthalimides in WSO and OSW, respectively.

2.5 Fluorescence titration

To further investigate the interactions of **3a** and **3b** with DNA, fluorescence titration experiments were carried out, in which the concentration of **3a** and **3b** is fixed at 10 μM. The changes in the emission were monitored by the titration of different concentration of DNA.

2.6 UV-Vis absorption titration of DNA with bisnaphthalimide

A typical titration of naphthalimide derivatives in HEPES buffer was performed by using a fixed concentration of 20 μM, to which the DNA stock solution was gradually added up to saturation. After each addition, the solution was mixed and allowed to re-equilibrate for 15 min before the absorption spectra were recorded. The binding constant K_a was determined from a $D/\Delta\varepsilon_{ap}$ vs D plot according to the following equation (eqn (2)) [44]:

$$D/\Delta\varepsilon_{ap} = D/\Delta\varepsilon + 1/[(\Delta\varepsilon)K_a] \quad (2)$$

where D is the concentration of DNA, $\Delta\varepsilon_{ap} = |\varepsilon_A - \varepsilon_F|$, $\varepsilon_A = A_{obs}/[\text{compound}]$, $\Delta\varepsilon = |\varepsilon_B - \varepsilon_F|$, and ε_B and ε_F correspond to the extinction coefficients of the DNA-compound adduct and unbound compound, respectively.

2.7 Circular dichroism (CD) studies

The oligonucleotides were dissolved in water to yield a 100 μM stock solution, and then diluted using 10 mM Tris-HCl (pH 7.4) with or without KCl. Prior to use in the CD assay, the DNA solution was annealed by heating to 95 °C for 5 min and slowly cooled to room temperature, and stored at 4 °C overnight. After that, 400 μL of 40 μM bisnaphthalimide was mixed with the annealed DNA. The final concentrations of oligonucleotides and bisnaphthalimides were 10 and 20 μM, respectively. The solution was incubated at room temperature for 2 h before examination.

2.8 Fluorescence resonance energy transfer (FRET) melting assay

The FRET experiments were carried out in 10 mM lithium cacodylate buffer (pH 7.2) containing 10 mM KCl and 90 mM LiCl. The fluorescently labeled oligonucleotide strand FHtelo (5'-FAM-GGG-TTA-GGG-TTA-GGG-TTA-GGG-TAMRA-3') and Fmyc

(5'-FAM-TTG-AGG-GTG-GGT-AGG-GTG-GGT-AA-TAMRA-3') were used as the FRET probe, in which FAM and TAMRA was 6-carboxyfluorescein and 6-carboxytetramethylrhodamine, respectively. FHtelo and Fmyc were diluted from 20 μM stock solution to 0.2 μM, and then annealed by heating to 90 °C for 5 min, followed by slowly cooling to room temperature. After that, bisnaphthalimides were mixed with the annealed fluorescently labeled oligonucleotide. The final concentrations of fluorescently labeled oligonucleotide and bisnaphthalimides were 0.2 and 1.0 μM, respectively. Measurements were performed on a Hitachi F-4600 with excitation at 492 nm and detection at 516 nm. The temperature of the solution was increased from 27 to 96 °C at intervals of 0.5 °C/min, maintaining a constant temperature of 3 min before each measurement. Final analysis of the data was carried out using Origin 9.0 (OriginLab Corp.). The melting results were the average of two replicates.

2.9 Molecular docking studies

Docking studies were carried out using AutoDock (Version 4.2). The bisnaphthalimides were optimized by Density Functional Theory (DFT/B3LYP) method with 6-31G basis sets. The optimized structures were used to do the docking. The crystal structures of the telomeric, c-myc and c-kit G-quadruplexes were obtained from the Protein Data Bank (PDB). AutoDock Tools 1.5.6 was used to establish the Autogrid points and to visualize the docked structure of G-quadruplex-ligand complex. In order to explore the entire conformation of nucleic acids, the 3D grid box dimensions had been defined including the entire DNA macromolecules.

2.10 Fluorescence imaging

For the purpose of staining and imaging, A549 cells were seeded onto 35 mm cell culture dishes and cultured for 24 h (cell confluence must be over 80%). The cells were incubated with naphthalimides and/or DAPI for 2 h. The unbound molecules were washed three times with PBS. Cells were imaged using an Olympus IX70 fluorescence microscope (Olympus Corporation, Japan). The fluorescence of DAPI was excited by a 405 nm laser and collected from 425 to 475 nm; the fluorescence of naphthalimides was excited by a 488 nm laser and collected from 500 to 600 nm. Florescent images were processed using the Olympus FV10-ASW 1.6 viewer software.

2.11 Cytotoxicity assay

All tissue culture media and reagents were obtained from Hy-Clone, Thermo Scientific A549 and normal human lung fibroblast MRC-5 cells were maintained in bulbecco's modified eagle medium (DMEM) containing 10% fetal bovine serum. A549 and MRC-5 cells were plated at 2×10^5 per well in a Nunc 48 well plate and allowed to grow for 24 h. The cells were exposed to increasing concentrations of bisnaphthalimides and incubated for 48 h. The loading medium was then removed and the cells were fed with medium containing MTT. Cell viability was then measured by reading the absorbance at 570 nm using a Thermo MK3 Multiscan microplate reader. The signal was normalized to 100% viable (untreated) cells. Growth inhibition by bisnaphthalimides was evaluated by IC_{50} (concentration of a drug causing 50% inhibition of cell growth). Each growth inhibition experiment was repeated at least three times and the results were expressed as mean ± standard deviation (SD).

3. Results and Discussion

3.1 Synthesis and photophysical properties of bisnaphthalimides

The bisnaphthalimides have been known to possess strong DNA-binding affinity and anticancer activity [45,46]. In the present study, four bisnaphthalimides **3a**, **3b**, **5a** and **5b** are synthesized (Scheme 1). Reaction of 4-bromo-1,8-naphthalic anhydride with morpholine in the presence of 2-ethoxyethanol affords compound **2**. The bisnaphthalimides **3a** is synthesized by the reaction of the corresponding polyamine N,N-bis(2-aminoethyl)propane-1,3-diamine and **2** in a 1:2 ratio. The compound **3a** can be converted to **3b** by reductive amination with formaldehyde.

Reaction of 4-bromo-1,8-naphthalic anhydride with sodium azide results in 4-azido-1,8-naphthalic anhydride. Click reaction of ethynylbenzene with 4-azido-1,8-naphthalic anhydride is performed in DMF at 60 °C for 14 h, affording **4**. The bisnaphthalimides 5a and 5b are synthesized according to a similar procedure as that of **3a** and **3b**. The lipophilicity (logP) increases in the order of **3a** (0.45) < **5a** (0.60) < **3b** (0.67) < **5b** (0.89), demonstrating that N-methylation of the linkage can enhance the lipophilicity of bisnaphthalimide [47]. All these compounds are isolated and purified by flash chromatography on silica gel, and are structurally characterized by ^{1}H NMR, ^{13}C NMR and mass spectrometry (Fig. S1-S12).

The spectroscopic properties of **3a**, **3b**, **5a** and **5b** in various solvents, including THF, ethanol and HEPES buffer, are summarized in Table 1. In THF, the absorption spectra of **3a** and **3b** display two bands centered at 258 and 387 nm, and the emission spectra show a peak around 512 nm (Fig.S13). The emission spectra of **3a** and **3b** are red shifted in polar solvents (Fig.S13b and Table 1), which can be attributed to the intramolecular charge transfer (ICT) between the morpholine group and the naphthalimide ring system [48]. For the triazole derivatives **5a** and **5b**, the absorption spectra and the emission spectrum are slightly affected by the solvent polarity, indicating relatively low charge transfer efficiency between triazole and naphthalimide moiety

[49,50].

The quantum yields of **3a** and **3b** are moderate in THF (Table 1), and decrease dramatically in polar solvents. On the other hand, **5a** and **5b** are weakly fluorescent in all solvents. These results indicate that the substituent groups at the 4-position can affect the photophysical properties of bisnaphthalimides.

3.2 UV-Vis absorption titration studies

It is well known that the naphthalimides are capable of binding to duplex DNA through the major groove and/or *via* intercalation interaction. The interaction of **3a**, **3b**, **5a** and **5b** with different DNA samples is investigated by absorption spectroscopy. In HEPES buffer solution containing 100 mM KCl, the addition of CT DNA to the solution of **3a** and **3b** leads to considerable hypochromicity (Fig. 1). By using a plot of $D/\Delta\varepsilon_{ap}$ versus D (Fig. 1a insets) according to the Scatchard equation, the binding affinity (K_a) toward CT DNA can be determined. The results are summarized in Table 2. The K_a values of **3a**, **3b** and **5b** with CT DNA are in the range of 5.72×10^4~1.08×10^5 M^{-1}, similar to that of the 4-substituted bisnaphthalimide [51]. No obvious spectral shift can be observed in such system, suggesting that these bisnaphthalimides bind with CT DNA through groove interaction. As for **5a**, addition of CT DNA leads to weak decrease in the absorbance (within 5%), indicating weak interaction between **5a** and CT DNA (Fig.S14).

Upon incremental addition of the preannealed Htelo, c-myc and c-kit G4s, the absorption spectra of **3a**, **3b** and **5b** show 12.9~44.0% hypochromism without obvious red shift, indicating that **3a**, **3b** and **5b** interact with G4 through external binding mode (Fig. S15-S17). As shown in Table 2, **3a**, **3b** and **5b** show high affinity toward Htelo, c-myc and c-kit G4s ($K_a > 4.42\times10^6$ M^{-1}),

comparable to those of reported good quadruplex binders, such as platinum complex, ruthenium complex, tetraazaperopyrene, phthalocyanine and phenanthroline derivatives [52-55]. The compounds **3a**, **3b** and **5b** exhibit more than 40-fold selectivity for quadruplexes versus duplex in the presence of potassium, similar to that of Pt(II) complexes [56]. As for **5a**, it also shows good affinity toward Htelo and c-kit quadruplexes, but low affinity toward c-myc (Table 2, Fig. S16c). These results suggest that subtle structure modification, such as N-methylation of linkage, can affect the binding affinity of bisnaphthalimides with G4s.

3.3 Fluorescence titration studies

We investigated the changes in fluorescence of **3a** and **3b** in the presence of G-quadruplexes, as well as CT DNA. Fig. 2a presents the steady-state fluorescence spectra of **3a** in the presence of different amount of c-myc. In the absence of c-myc, **3a** is weakly fluorescent in buffer solution. Upon addition of c-myc, the fluorescence intensity increases gradually, with an increase of about 27.2-fold eventually. As for **3b**, addition of c-myc also leads to a fluorescence enhancement of about 20.2-fold at saturation (Fig. 2b). The emission peaks blue-shift obviously with the addition of G4 DNA, suggesting that the naphthalimide moiety of **3a** and **3b** may penetrate into the hydrophobic environment of G-quadruplex (Fig.S18-19) [57]. The titration curves with different DNA reveal that the degree of fluorescence enhancement strongly depends on the types of DNA (Fig. 2c and 2d). The telomeric and oncogenic G-quadruplexes induce strong enhancement of the fluorescence intensity (18 to 27-fold, Table 3), whereas the duplex CT DNA induces much weaker fluorescence enhancement (around 2-fold). In contrast to the linear structure of double-stranded DNA, intramolecular G4s are globular structures derived from the sequence-dependent folding of single-stranded DNA. The special structural characteristics make **3a** and **3b** interact with G4s with

high selectivity [58,59]. These results indicate that **3a** and **3b** can serve as a light-up fluorescent probe with good sensitivity and excellent selectivity toward G-quadruplex over duplex DNA (Fig. S20). For **5a** and **5b**, the addition of G-quadruplex and duplex DNA results in a much smaller enhancement, maybe due to the low fluorescence quantum yield of **5a** and **5b** in organic solvents and buffer solution (Fig. S21).

3.4 Circular dichroism (CD) spectra studies

The CD spectroscopic studies are carried out to assess the structural changes of G-quadruplexes upon interaction with **3a**, **3b**, **5a** and **5b**. In the presence of K^+ ions, c-myc and c-kit exhibit a parallel structure, with a positive band at 265 nm and a negative band at 240 nm (Fig. 3a and Fig. S22a) [60]. The CD spectra of c-myc and c-kit are almost unaffected upon addition of **3a**, **3b**, **5a** and **5b**, indicating that c-myc and c-kit maintain their conformations upon interaction with **3a**, **3b**, **5a** and **5b**. In the case of Htelo, it shows a strong positive band at 295 nm, with two weak positive peaks at 250 and 270 nm (Fig. 3b), characteristic of mixed parallel/antiparallel-stranded G-quadruplex structure [61]. Compounds **3a**, **5a**, and **5b** induce a comparable stabilization of the mixed–hybrid structure as proved by the increase in the positive peaks at 290 and 270 nm. However, addition of **3b** leads to an increase in the positive band around 290 nm and an obvious decrease in the positive band at 250 nm, suggesting **3b** can convert Htelo into antiparallel G-quadruplex [62].

In the absence of K^+ ions, c-myc, Htelo and c-kit exhibit two positive peaks at about 255 and 295 nm (Fig. 3c-d and Fig. S22b), indicating the coexistence of unfolded sequence and quadruplex structure [63]. For c-kit, the peak position of the band remains unchanged upon addition of **3a**, **3b**, **5a** and **5b**, suggesting that these compounds could not induce the formation of c-kit quadruplex

(Fig. S22b). As for c-myc, the positive peak at 265 nm is enhanced, and a negative peak at 240 nm appears when interacting with **3a** and **3b** and **5b**, suggesting that the parallel structure of c-myc can be induced by **3a**, **3b** and **5b** (Fig. 3c) [64]. Regarding Htelo, the intensity of the positive band at 295 nm increases and a negative band at 265 nm appears upon addition of **3a**, **3b** and **5b,** suggesting that **3a**, **3b** and **5b** can efficiently induce the formation of antiparallel quadruplex (Fig. 3d) [56]. On the other hand, the CD spectra of c-myc and Htelo show some changes after addition of **5a**. However, the resulting CD spectra are different from the characteristic CD spectra of parallel c-myc quadruplex and antiparallel telomeric quadruplex. No induced CD spectra (ICD) can be observed in the range of 300-400 nm, indicating that **3a**, **3b**, **5a** and **5b** may interact with c-myc, Htelo and c-kit through external binding mode [65].

3.5 Molecular docking studies

To gain further insight into the binding mode of **3a**, **3b**, **5a** and **5b** with the G-quadruplex, Molecular docking studies are carried out [66]. The X-ray crystal structures of the telomeric (PDB ID: 1KF1), c-myc (PDB ID: 1XAV) and c-kit (PDB ID: 2O3M) are docked with the DFT optimized molecular structures of **3a**, **3b**, **5a** and **5b** using AutoDock 4.2. The docking results of **3a**, **3b**, **5a** and **5b** in various binding site of G4s are showing in Fig. S23-25. These bisnaphthalimides mainly bind in the groove and/or loop region of the G4s, in agreement with the UV-Vis titration and CD experimental results. The representative docking results are shown in Fig. 4-5 and S26.

For the telomeric G-quadruplex (PDI ID: 1FK1), the best docked poses of **3a**, **3b**, **5a** and **5b** have been shown in Fig. 4. The naphthalimide moieties of **3a** and **3b** are directed into the channel formed between the TTA loop and G-tetrad. Hydrogen bond is formed between quadruplex and

the polyamine linkage in **3a** or the carbonyl groups in **3b** (Fig. 4a-b). The naphthalimide moiety of **3b** can enter the loop more deeply than that of **3a**, which may arise from the larger lipophilicity of **3b** than **3a** [67]. Similarly, the naphthalimide moiety of **5b** can penetrate into the loop of Htelo, while that of **5a** can't (Fig. 4c-d). The triazole side-chains of **5a** and **5b** are properly directed into the DNA grooves and filled the groove space, which may help lock the ligand onto the G-quadruplex. The triazole moiety in **5a** and **5b** interacts with the groove through hydrogen bond [68]. These results suggest that the increase in the lipophilicity by N-methylation of the linkages can affect the binding model of bisnaphthalimides with G-quadruplex.

In the case of c-myc quadruplex (PDB ID: 1XAV), there are three loops bridging three G-tetrad layers and connecting adjacent parallel strands [69]. The best docked poses of **3a**, **3b** and **5b** have been shown in Fig. 5. Hydrogen bonds are formed between c-myc quadruplex and the polyamine linkage in **3a**, **3b** and the triazole moiety in **5b**, respectively. The docking results also show that hydrogen bond exists between bisnaphthalimides and c-kit quadruplex (Fig. S24 and Fig. S26).

3.6 FRET melting assay

The ability of bisnaphthalimides **3a**, **3b**, **5a** and **5b** to stabilize the G-quadruplex is further evaluated by the FRET-melting assay. As shown in Fig. 6a, **3a** and **3b** appear as relatively strong telomeric G-quadruplex stabilizers, with an increase in the melting temperature (ΔT_m) of around 10 ℃ (Table 4). In contrast, the ΔT_m induced by **5a** and **5b** is around 3 ℃. For c-myc, a moderate increase in T_m values (ΔT_m ~4.7–7.4 ℃) is obtained after the addition of **3a**, **3b** and **5b** (Fig. 6b). Addition of **5a** results in a small change in the T_m (–0.3 ℃), suggesting that **5a** weakly interacts with c-myc G-quadruplex. The compounds **3a** and **3b** possess good interaction properties

with G4 strands, with similar change in melting temperature of the G4s as that of polyaromatic compounds [15] and previous reported mono-naphthalimides [28-31].

3.7 Cellular location studies

Being fluorescent, it is convenient to track the cellular localization of **3a** and **3b** by fluorescence imaging. Fluorescence microscopy is used to study the localization of **3a** and **3b** in A549 lung carcinoma cells. A convenient and reliable DNA-specific nuclear stain, DAPI is chosen for costaining. As shown in Fig. 7, after incubation at 37 °C for 2 h, **3a**, **3b** and DAPI have entered living cells. The green fluorescence of **3a**, **3b** and blue fluorescence of DAPI are observed. The merged images show that **3a** and **3b** can readily be taken up by A549 lung cancer cells, but not just localize in the nucleus.

3.8 Cytotoxicity of bisnaphthalimides

The cytotoxicity of **3a**, **3b**, **5a** and **5b** against non-small cell lung cancer cell line A549 and noncancerous cells MRC-5 is assessed using the MTT assay (Fig. S27a). As shown in Table 5, **3a**, **3b**, **5a** and **5b** show good anticancer activities against the A549 cell lines, with the IC_{50} values in the range of 0.15 to 1.04 μM. All the compounds are more effective in killing A549 cancer cells than the standard drug amonafide. In particular, **3b** is up to 25 times more effective in killing A549 cells than the reference drug. Importantly, **3a**, **3b**, **5a** and **5b** exhibit significantly less cytotoxicity against a noncancerous human embryonic lung fibroblast cells MRC-5 cells (Fig. S27b), with the IC_{50} values in the range of 0.95 μM to 2.22 μM. These results indicate that **3a**, **3b**, **5a** and **5b** are promising anti-proliferative agents.

4. Conclusion

In conclusion, four bisnaphthalimides have been investigated for their potential G-quadruplex

binding. The compounds **3a**, **3b** and **5b** display high affinity for telomeric and oncogenic G-quadruplexes. On the other hand, **5a** only show high affinity for the c-kit and telomeric quadruplex ($K_a > 10^6$ M^{-1}), and interact with c-myc quadruplex and duplex CT DNA weakly. Molecular docking analysis suggests that **3a**, **3b**, **5a** and **5b** interact with the groove and/or loop of the G-qudruplex through hydrogen bonding. Fluorescence intensity of **3a** and **3b** is enhanced dramatically in the presence of G-quadruplex. Fluorescence imaging further indicate that **3a** and **3b** can readily enter A549 cells. These compounds efficiently inhibit the growth of A549 cancer cell lines with low cytotoxicity toward noncancerous cell MRC-5. These results indicate that the bisnaphthalimide with G-quadruplex binding properties may possess tumor cell-selective cytotoxic activity, which is helpful to design novel naphthalimide anticancer agent.

Acknowledgements

This research is supported by the Natural Science Foundation of Shaanxi Province (2018JM2019, 2016JM2013), the National Natural Science Foundation of China (21073143), and the NPU Foundation for Graduate Innovation (ZZ2017192).

Supporting Information Available

Supplementary absorption spectra, fluorescence spectra, CD spectra, Autodock analysis results, and copies of NMR spectra and Mass spectra are included.

References

[1] A.T. Phan, Y.S. Modi, D.J. Patel, Propeller-type parallel-stranded G-quadruplexes in the human c-myc promoter, J. Am. Chem. Soc. 126 (2004) 8710−8716.

[2] J.L. Huppert, S. Balasubramanian, Prevalence of quadruplexes in the human genome, Nucleic Acids Res. 33 (2005) 2908−2916.

[3] D. Wei, J. Husby, S. Neidle, Flexibility and structural conservation in a c-KIT G-quadruplex, Nucleic Acids Res. 43 (2015) 1629−644.

[4] G. Guilbaud1, P. Murat, B. Recolin1, B.C. Campbell, A. Maiter1, J.E. Sale1, S. Balasubramanian, Local epigenetic reprogramming induced by G-quadruplex ligands,

Nat. Chem. 9 (2017) 1110−1117.

[5] M.C. Chen, R. tippana, N.A. Demeshkina, P. Murat, S. Balasubramanian, S. Myong, A.R. Ferre-D'Amare, Structural basis of G-quadruplex unfolding by the DEAH/RHA helicase DHX36, Nature 558 (2018) 465−469.

[6] Y. Lu, T. Ou, J. Tan, J. Hou, W. Shao, D. Peng, N. Sun, X. Wang, W. Wu, X. Bu, Z. Huang, D. Ma, K. Wong, L. Gu, 5-N-Methylated quindoline derivatives as telomeric G-quadruplex stabilizing ligands: effects of 5-N positive charge on quadruplex binding affinity and cell proliferation, J. Med. Chem. 51 (2008) 6381−6392.

[7] N. Meyer, L.Z. Penn, Reflecting on 25 years with MYC, Nat. Rev. Cancer 8 (2008) 976−990.

[8] S. Pelengaris, M. Khan, G. Evan, c-MYC: more than just a matter of life and death, Nat. Rev. Cancer 2 (2002) 764−776.

[9] A. Siddiqui-Jain, C.L. Grand, D.J. Bearss, L.H. Hurley, Direct evidence for a G-quadruplex in a promoter region and its targeting with a small molecule to repress c-MYC transcription, Proc. Natl. Acad. Sci. USA 99 (2002) 11593−11598.

[10] L. Li, J. Lu, W. Zhou, H. Li, X. Yang, Studies on the interaction mechanism of aminopyrene derivatives with human tumor-related DNA, J. Photochem. Photobiolo. B: Biol. 123 (2013) 32−40.

[11] M. Debnath, S. Ghosh, A. Chauhan, R. Paul, K. Bhattacharyya, J. Dash, Preferential targeting of i-motifs and G-quadruplexes by small molecules, Chem. Sci. 8 (2017) 7448−7456.

[12] G. Hao, J. Sun, C. Wei, Studies on interactions of carbazole derivatives with DNA, cell image, and cytotoxicity, Bioorg. Med. Chem. 26 (2018) 285−294.

[13] I. Buchholz, B. Karg, J. Dickerhoff, A. Sievers-Engler, M. Lammerhofer, K. Weisz, Selective targeting of G-quadruplex structures by a benzothiazole-based binding motif, Chem. Eur. J. 23 (2017) 5814−5823.

[14] A. Chauhan, R. Paul, M. Debnath, I. Bessi, S. Mandal, H. Schwalbe, J. Dash, Synthesis of fluorescent binaphthyl amines that bind c-MYC G-quadruplex DNA and repress c-MYC expression, J. Med. Chem. 59 (2016) 7275−7281.

[15] A. Ou, A. Guedin, B.W. Skelton, S. Amrane, C.W. Evans, M. Norret, K.S. Iyer, J.

Mergny, N.M. Smith, Multicarbazole scaffolds for selective G-quadruplex binding, Chem. Commun. 54 (2018) 9647−9650.

[16] A. Leczkowska, J. Gonzalez-Garcia, C. Perez-Arnaiz, B. Garcia, A.J.P. White, R. Vilar, Binding studies of metal salphen and metal bipyridine complexes towards G-quadruplex DNA, Chem. Eur. J. 24 (2018) 11785−11794.

[17] H. Xu, M.D. Antonio, S. McKinney, V. Mathew, B. Ho, N.J. O'Neil, N.D. Santos, J. Silvester, V. Wei, J. Garcia, F. Kabeer, D. Lai, P. Soriano, J. Banath, D.S. Chiu, D. Yap, D.D. Le, F.B. Ye, A. Zhang, K. Thu, J. Soong, S. Lin, A.H.C.Tsai, T. Osako, T. Algara, D.N. Saunders, J. Wong, J. Xian, M.B. Bally, J.D. Brenton, G.W. Brown, S.P. Shah, D. Cescon, T.W. Mak, C. Caldas, P.C. Stirling, P. Hieter, S. Balasubramanian, S. Aparicio, CX-5461 is a DNA G-quadruplex stabilizer with selective lethality in BRCA1/2 deficient tumours, Nat. Coomun. 2017 (8) 14432.

[18] S. Bandeira, J. Gonzalez-Garcia, E. Pensa, T. Albrecht, R. Vilar, A redox-activated G-quadruplex DNA binder based on a platinum(IV)–salphen complex, Angew. Chem. 130 (2018) 316−319.

[19] T.P. Pradeep, R. Barthwal, A 4:1 stoichiometric binding and stabilization of mitoxantrone-parallel stranded G-quadruplex complex established by spectroscopy techniques, J. Photochem. Photobiol. B: Biol. 162 (2016) 106−114.

[20] C. Lin, G. Wu, K. Wang, B. Onel, S. Sakai, Y. Shao, D. Yang, Molecular recognition of the hybrid-2 human telomeric G-quadruplex by epiberberine: insights into conversion of telomeric G-quadruplex structures, Angew. Chem. Int. Ed. 57 (2018) 10888−10893.

[21] M.F. Brana, A. Ramos, Naphthalimides as anti-cancer agents: synthesis and biological activity, Curr. Med. Chem. Anti-Cancer Agents 1 (2001) 237−255.

[22] K. Wang, Y. Wang, X. Yan, H. Chen, G. Ma, P. Zhang, J. Li, X. Li, J. Zhang, DNA binding and anticancer activity of naphthalimides with 4-hydroxyl-alkylamine side chains at different lengths, Bioorg. Med. Chem. Lett. 22 (2012) 937−941.

[23] Z. Li, Q. Yang, X. Qian, Synthesis, antitumor evaluation and DNA photocleaving activity of novel methylthiazonaphthalimides with aminoalkyl side chains, Bioorg. Med. Chem. Lett. 15 (2005) 3143−3146.

[24] Q. Yang, P. Yang, X. Qian, L. Tong, Naphthalimide intercalators with chiral amino side

chains: effects of chirality on DNA binding, photodamage and antitumor cytotoxicity, Bioorg. Med. Chem. Lett. 18 (2008) 6210−2613.

[25] M. Verma, V. Luxami, K. Paul, Synthesis, in vitro evaluation and DNA interaction studies of N-allyl naphthalimide analogues as anticancer agents, RSC Adv. 5 (2015) 41803−41813.

[26] S. Tan, D. Sun, J. Lyu, X. Sun, F. Wu, Q. Li, Y. Yang, J. Liu,X. Wang, Z. Chen, H. Li, X. Qian, Y. Xu, Antiproliferative and apoptosis-inducing activities of novel naphthalimide–cyclam conjugates through dual topoisomerase (topo) I/II inhibition, Bioorg. Med. Chem. 23 (2015) 5672–5680.

[27] C. Bailly, C. Carrasco, A. Joubert, C. Bal, N. Wattez, M.P. Hildebrand, A. Lansiaux, P. Colson, C. Houssier, M. Cacho, A. Ramos, M.F. Brana, Chromophore-modified bisnaphthalimides: DNA recognition, topoisomerase inhibition, and cytotoxic properties of two mono- and bisfuronaphthalimides, Biochemistry 42 (2003) 4136−4150.

[28] A. Peduto, B. Pagano, C. Petronzi, A. Massa, V. Esposito, A. Virgilio, F. Paduano, F. Trapasso, F. Fiorito, S. Florio, C. Giancola, A. Galeone, R. Filosa, Design, synthesis, biophysical and biological studies of trisubstituted naphthalimides as G-quadruplex ligands, Bioorg. Med. Chem. 19 (2011) 6419−6429.

[29] Y. Gao, W. Cai, Z. Ou, T. Ma, N. Yi, Z. Li, DNA interactions and cytotoxicity of imidazole-modified naphthalimides, Acta Phys-Chim. Sin. 35 (2019) 230-240.

[30] Z. Ou, Y. Qian, Y. Gao, Y. Wang, G. Yang, Y. Li, K. Jiang, X. Wang, Photophysical, G-quadruplex DNA binding and cytotoxic properties of terpyridine complexes with a naphthalimide ligand, RSC Adv. 6 (2016) 36923−36931.

[31] Z. Ou, M. Xu, Y. Gao, R. Hu, Q. Li, W. Cai, Z. Wang, Y. Qian, G. Yang, Synthesis, G-quadruplex binding properties and cytotoxicity of naphthalimide thiourea conjugates, New J. Chem. 41 (2017) 9397−9405.

[32] S. Banerjee, E.B. Veale, C.M. Phelan, S.A. Murphy, G.M. Tocci, L.J. Gillespie, D.O. Frimannsson, J.M. Kelly, T. Gunnlaugsson, Recent advances in the development of 1,8-naphthalimide based DNA targeting binders, anticancer and fluorescent cellular imaging agents, Chem. Soc. Rev. 42 (2013) 1601−1618.

[33] C. Bailly, M. Brana, M.J. Waring, Sequence-selective intercalation of antitumour

bis-naphthalimides into DNA, Febs J. 240 (2010) 195−208.

[34] K. Suzuki, H. Nagasawa, Y. Uto, Y. Sugimoto, K. Noguchi, M. Wakida, K. Wierzba, T. Terada, T. Asao, Y. Yamada, Napthalimidobenzamide DB-51630: a novel DNA binding agent inducing p300 gene expression and exerting a potent anti-cancer activity, Bioorg. Med. Chem. 13 (2005) 4014−4021.

[35] M.F. Brana, M. Cacho, M.A. Garcia, B. de Pascual-Teresa, A. Ramos, M.T. Dominguez, J.M. Pozuelo, C. Abradelo, M.F. Rey-Stolle, M. Yuste, M. Banez-Coronel, J.C. Lacal, New analogues of Amonafide and Elinafide, containing aromatic heterocycles: synthesis, antitumor activity, molecular modeling, and DNA binding properties, J. Med. Chem. 47 (2004) 1391−1399.

[36] J. Gallego, B.R. Reid, Solution structure and dynamics of a complex between DNA and the antitumor bisnaphthalimide LU-79553: intercalated ring flipping on the millisecond time scale, Biochemistry 38 (1999) 15104−15115.

[37] S. Shanmugaraju, B.C. Poulsen, T. Arisa, D. Umadevi, H.L. Dalton, C.S. Hawes, S. Estalayo-Adrian, A.J. Savyasachi, G.W. Watson, D.C. Williamsd, T. Gunnlaugsson, Synthesis, structural characterisation and antiproliferative activity of a new fluorescent 4-amino-1,8-naphthalimide Troger's base–Ru(II)–curcumin organometallic conjugate, Chem. Commun. 54 (2018) 4120−4123.

[38] Y. Huang, C. Wu, Y. Song, M. Huang, D. Tian, X. Yang, Y. Fan, Synthesis, DNA binding, and anticancer properties of bis-naphthalimide derivatives with lysine-modified polyamine linkers, Molecules 23 (2018) 266.

[39] H. Sun, J. Xiang, Y. Liu, L. Li, Q. Li, G. Xu, Y. Tang, A stabilizing and denaturing dual-effect for natural polyamines interacting with G-quadruplexes depending on concentration, Biochimie 93 (2011) 1351−1356.

[40] D. Panda, P. Saha, T. Das, J. Dash, Target guided synthesis using DNA nano-templates for selectively assembling a G-quadruplex binding c-MYC inhibitor, Nat. Commun. 8 (2017) 16103.

[41] C. Marchetti, K.G. Zyner, S.A. Ohnmacht, M. Robson, S.M. Haider, J.P. Morton, G. Marsico, T. Vo, S. Laughlin-Toth, A.A. Ahmed, G.D. Vita, I. Pazitna, M. Gunaratnam, R.J. Besser, A.C.G. Andrade, S. Diocou, J.A. Pike, D. Tannahill, R.B. Pedley, T.R.J.

Evans, W.D. Wilson, S. Balasubramanian, S. Neidle, Targeting multiple effector pathways in pancreatic ductal adenocarcinoma with a G-Quadruplex-binding small molecule, J. Med. Chem. 61 (2018) 2500−2517.

[42] J.V. Morris, M.A. Mahaney, J.R. Hube, Fluorescence quantum yield determinations. 9,10-Diphenylanthracene as a reference standard in different solvents, J. Phys. Chem. 80 (1976) 969−974.

[43] X. Li, Y. Lin, Q. Wang, Y. Yuan, H. Zhang, X. Qian, The novel anti-tumor agents of 4-triazol-1,8-naphthalimides: synthesis, cytotoxicity, DNA intercalation and photocleavage, Eur. J. Med. Chem. 46 (2011) 1274−1279.

[44] A. Wolfe, Jr G.H. Shimer, T. Meehan, Polycyclic aromatic hydrocarbons physically intercalate into duplex regions of denatured DNA, Biochemistry 26 (1978) 6392−6396.

[45] M.F. Brana, M. Cacho, A. Ramos, M.T. Dominguez, J.M. Pozuelo, C. Abradelo, M.F. Rey-Stolle, M. Yuste, C. Carrasco, C. Bailly, Synthesis, biological evaluation and DNA binding properties of novel mono and bisnaphthalimides, Org. Biomol. Chem. 1 (2003) 648−654.

[46] G.A. Barron, M. Goua, I. Kuraoka, G. Bermano, S. Iwai, P.K.T. Lin, Bisnaphthalimidopropyl diaminodicyclohexylmethane induces DNA damage and repair instability in triple negative breast cancer cells via p21 expression, Chem-Biol. Interact. 242 (2015) 307−315.

[47] S.M.A. Rauf, P.I. Arvidsson, F. Albericio, T. Govender, G.E.M. Maguire, H.G. Kruger, B. Honarparvar, The effect of N-methylation of amino acids (Ac-X-OMe) on solubility and conformation: a DFT study, Org. Biomol. Chem. 13 (2015) 9993–10006.

[48] J. Zhou, H.Y. Liu, B. Jin, X.J. Liu, H.B. Fu, D.H. Shangguan, A guanidine derivative of naphthalimide with excited-state deprotonation coupled intramolecular charge transfer properties and its application, J. Mater. Chem. C 1 (2013) 4427−4436.

[49] G.R. Bardajee, A.Y. Li, J.C. Haley, M.A. Winnik, The synthesis and spectroscopic properties of novel, functional fluorescent naphthalimide dyes, Dyes Pigment. 79 (2008) 24−32.

[50] E. Jang, T. Ding, M. Xie, H. Cao, Investigation of photophysical properties of 1,8-naphthalimides with an extended conjugation on naphthalene moiety via Suzuki

coupling reaction, J. Photochem. Photobiology A: Chem. 364 (2018) 145−150.

[51] R. Rong, S. Wang, X. Liu, R. Li, K. Wang, Z. Cao, X. Li, Lysosomes-targeting imaging and anticancer properties of novel bis-naphthalimide derivatives, Bioorg. Med. Chem. Lett. 28 (2018) 742−747.

[52] S. Gam, I. Rodrigues, F. Mendes, I.C. Santos, E. Gabano, B. Klejevskaja, J. Gonzalez-Garcia, M. Ravera, R. Vilar, A. Paulo, Anthracene-terpyridine metal complexes as new G-quadruplex DNA binders, J. Inorg. Biochem. 160 (2016) 275−286.

[53] L. Hahn, N.J. Buurma, L.H. Gade, A water-soluble tetraazaperopyrene dye as strong G-quadruplex DNA binder, Chem. Eur. J. 22 (2016) 6314−6322.

[54] E. Bagda, E. Bagda, M. Durmus, G-quadruplex and calf thymus DNA interaction of quaternized tetra and octa pyridyloxy substituted indium (III) phthalocyanines, J. Photochem. Photobiol. B: Biol. 175 (2017) 9−19.

[55] L. Rao, J.D. Dworkin, W.E. Nell, U. Bierbach, Interactions of a platinum-modified perylene derivative with the human telomeric G-Quadruplex, J. Phys. Chem. B 115 (2011) 13701−13712.

[56] K. Suntharalingam, A.J.P. White, R. Vilar, Two metals are better than one: investigations on the interactions between dinuclear metal complexes and quadruplex DNA, Inorg. Chem. 49 (2010) 8371−8380.

[57] Z. Ou, B. Ju, Y. Gao, Z. Wang, G. Huang, Y. Qian, Alkynylplatinum(II) 2,6-bis(n-ethylbenzimidazol-2'-yl)pyridine complexes: effect of alkynyl ligand on G-quadruplex binding properties and anticancer activity, Acta Phys-Chim. Sin. 31 (2015) 2386−2394.

[58] H. Chen, H. Sun, Y. Chai, S. Zhang, A. Guan, Q. Li, L. Yao, Y. Tang, Insulin-like growth factor type I selectively binds to G-quadruplex structures, BBA - Gen. Subjects 1863 (2019) 31–38.

[59] B. Jin, X. Zhang, W. Zheng, X. Liu, C. Qi, F. Wang, D. Shangguan, Fluorescence light-up probe for parallel G-quadruplexes, Anal. Chem. 86 (2014) 943−952

[60] S. Burge, G.N. Parkinson, P. Hazel, A.K. Todd, S. Neidle, Survey and summary quadruplex DNA: sequence, topology and structure, Nucleic Acids Res. 34 (2006) 5402–5415.

[61] F. Doria, M. Nadai, M. Folini, M.D. Antonio, L. Germani, C. Percivalle, C. Sissi, N.

Zaffaroni, S. Alcaro, A. Artese, S.N. Richter, M. Freccero, Hybrid ligand–alkylating agents targeting telomeric G-quadruplex structures, Org. Biomol. Chem. 10 (2012) 2798–2806.

[62] H. Yu, L. Yu, Z. Hao, Y. Zhao, Interactions of ruthenium complexes containing indoloquinoline moiety with human telomeric G-quadruplex DNA, Spectrochim. Acta Part A Mol. Biomol. Spectrosc. 124 (2014) 187–193.

[63] P. Balagurumoorthy, S.K. Brahmachari, D. Mohanty, M. Bansal, V. Sasisekharan, Hairpin and parallel quartet structures for telomeric sequences, Nucleic Acids Res. 20 (1992) 4061–4067.

[64] M.W. Freyer, R. Buscaglia, K. Kaplan, D. Cashman, L.H. Hurley, E.A. Lewis, Biophysical studies of the c-MYC NHE III1 promoter: model quadruplex interactions with a cationic porphyrin, Biophys. J. 92 (2007) 2007−2015.

[65] V.S. Stafford, K. Suntharalingam, A. Shivalingam, A.J.P. White, D.J. Mann, R. Vilar, Syntheses of polypyridyl metal complexes and studies of their interaction with quadruplex DNA, Dalton Trans. 44 (2015) 3686−3700.

[66] Z. Ou, Y. Wang, Y. Gao, X. Wang, Y. Qian, Y. Li, X. Wang, Targeting human telomeric and c-myc G-quadruplexes with alkynylplatinum(II) terpyridine complexes under molecular crowding conditions, J. Inorg. Biochem. 166 (2017) 126–134.

[67] J. Li, X. Jin, L. Hu, J. Wang, Z. Su, Identification of nonplanar small molecule for G-quadruplex grooves: molecular docking and molecular dynamic study, Bioorg. Med. Chem. Lett. 21 (2011) 6969–6972.

[68] D. Zeng, G. Kuang, S. Wang, W. Peng, S. Lin, Q. Zhang, X. Su, M. Hu, H. Wang, J. Tan, Z. Huang, L. Gu, T. Ou, Discovery of novel 11-triazole substituted benzofuro[3,2-b]quinolone derivatives as c-myc G-Quadruplex specific stabilizers via click chemistry, J. Med. Chem. 60 (2017) 5407−5423.

[69] A. Ambrus, D. Chen, J. Dai, R.A. Jones, D. Yang, Solution structure of the biologically relevant G-quadruplex element in the human c-myc promoter. Implications for G-quadruplex stabilization, Biochemistry 244 (2005) 2048–2058.

Table 1 The photophysical properties of **3a**, **3b**, **5a** and **5b**

Compounds		λ_{abs} [nm] (ε [$\times 10^4$ L.mol^{-1}.cm^{-1}])	λ_{em} [nm] (Φ_{em})
3a	HEPES	409 (1.42)	547 (0.005)
	ethanol	394 (1.83)	532 (0.022)
	THF	258 (2.35), 387 (2.02)	512 (0.19)
3b	HEPES	408 (1.56)	546 (0.003)
	ethanol	388 (1.96)	531 (0.041)
	THF	258 (2.28), 387 (1.87)	512 (0.16)
5a	HEPES	355 (2.25)	406 (0.003)
	ethanol	345 (3.59)	388 (0.005)
	THF	246 (4.91), 345(3.81)	390 (0.012)
5b	HEPES	355 (2.04)	406 (0.002)
	ethanol	345 (3.36)	389 (0.003)
	THF	246 (4.48), 345 (3.41)	390 (0.012)

Table 2. Association constants (K_a, M^{-1}) of **3a**, **3b**, **5a** and **5b** with CT DNA, Htelo, c-myc and c-kit determined by UV-Vis spectroscopy[a]

	3a	**3b**	**5a**	**5b**
CT DNA	8.75×10^4	1.08×10^5	N.D.	5.72×10^4
Htelo	6.86×10^6	6.60×10^6	7.55×10^6	4.42×10^6
c-myc	7.78×10^6	7.87×10^6	N.D.	1.99×10^7
c-kit	1.21×10^7	4.57×10^6	1.85×10^7	6.27×10^6
${}^{Htelo}K_a/{}^{CT\ DNA}K_a$	78.4	61.1	N.D.	77.3
${}^{c\text{-}myc}K_a/{}^{CT\ DNA}K_a$	88.9	72.9	N.D.	347.9
${}^{c\text{-}kit}K_a/{}^{CT\ DNA}K_a$	138.3	42.3	N.D.	109.6

[a]N.D. means not detected.

Table 3 Effects of double-stranded CT DNA and G-quadruplexes on the fluorescence enhancement (F/F_0) of naphthalimide derivatives[a]

DNA	**3a**	**3b**
c-myc	27.2	20.2
Htelo	25.2	20.7
ckit1	19.1	18.6
CT DNA	1.80	2.38

[a] The concentration of **3a**, **3b** is 10μM, and the concentration of DNA is 15 μM.

Table 4 FRET-melting assay results of **3a**, **3b**, **5a** and **5b** binding with G-quadruplex[a]

Compounds	ΔT_m[b]	
	FHtelo[c]	Fmyc[d]
3a	9.8	5.5
3b	10.3	7.4
5a	2.4	-0.3
5b	3.7	4.7

[a]The concentration of G-quadruplex and bisnaphthalimides are 0.2 and 1.0 μM, respectively. [b]ΔT_m means the difference in melting temperature. [c]ΔT_m = [T_m(FHtelo+compound) - T_m(FHtelo)]. T_m value of FHtelo is 52.7 ℃. [d]ΔT_m = [T_m(Fmyc+compound) - T_m(Fmyc)]. T_m value of Fmyc is 59.3 ℃.

Table 5 Antiproliferative activity of **3a**, **3b**, **5a** and **5b** in A549 and MRC-5 cell lines (IC_{50}, μM)[a]

compounds	$^{A549}IC_{50}$	$^{MRC\text{-}5}IC_{50}$
3a	0.51 ± 0.13	1.30 ± 0.23
3b	0.15 ± 0.03	0.95 ± 0.19
5a	0.89 ± 0.07	1.35 ± 0.43
5b	1.04 ± 0.07	2.22 ± 0.49
Amonafide	3.84 ± 0.31	0.99 ± 0.10

[a]Data are collected after 48 h of exposure to the drug.

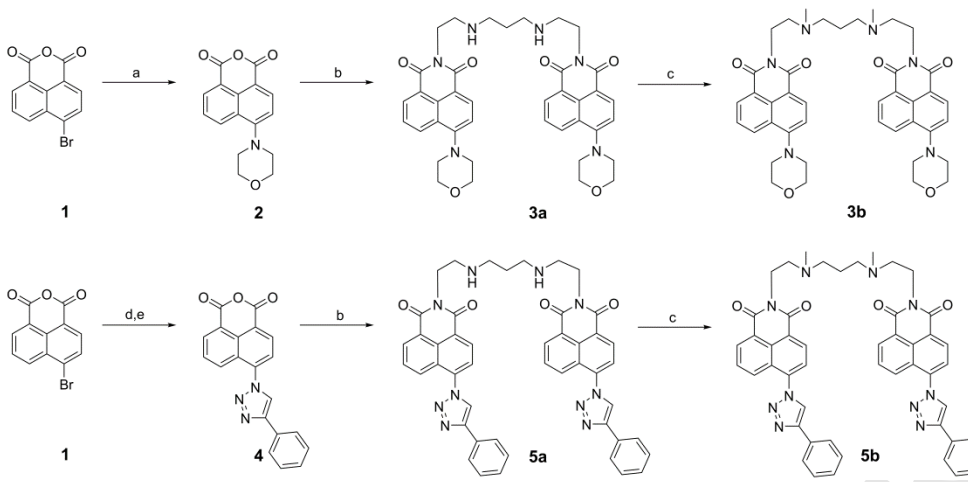

Scheme 1. Synthetic route of morpholine and triazole modified bisnaphthalimides. Reagents and conditions: (a) morpholine, 2-ethoxyethanol, reflux, 24 h; (b) N,N-bis(2-aminoethyl)propane-1,3-diamine, Et_3N, 1,4-dioxiane, reflux, 48 h; (c) CH_2O, AcOH, $NaBH_3CN$, MeOH, room temperature, 5 h; (d) NaN_3, NMP, 60 °C, 5 h; (e) ethynylbenzene, sodium ascorbate, $Cu(SO_4)\cdot 5H_2O$, DMF, 60 °C, 14 h.

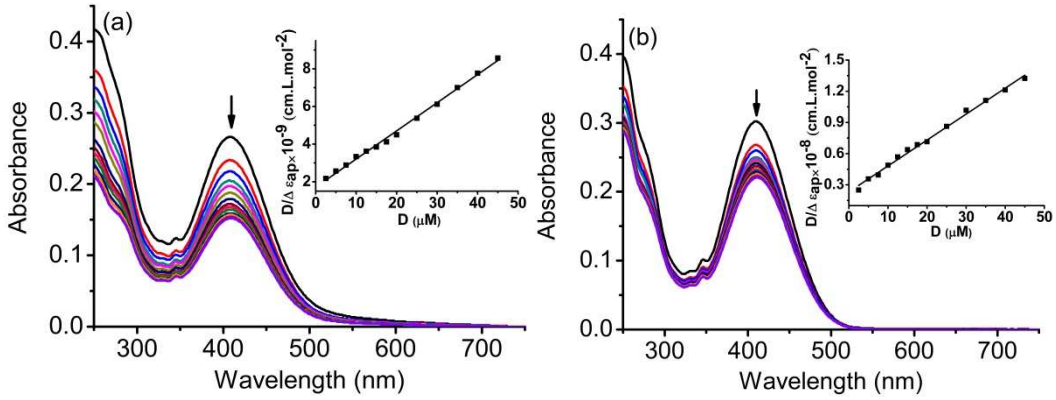

Fig. 1. UV-Vis titration of (a) **3a** and (b) **3b** with CT DNA in HEPES buffer (10 mM, pH 7.4) containing 0.1 M KCl. The arrows indicate the changes upon addition of DNA. Inset: Plot of $D/\Delta\varepsilon_{ap}$ versus D. D is the concentration of DNA, $\Delta\varepsilon_{ap} = |\varepsilon_A - \varepsilon_F|$. $\varepsilon_A = A_{obs}/[\text{naphthalimide}]$, ε_F corresponds to the extinction coefficients of the unbound nanphthalimides. [**3a**] = [**3b**] = 20 μM.

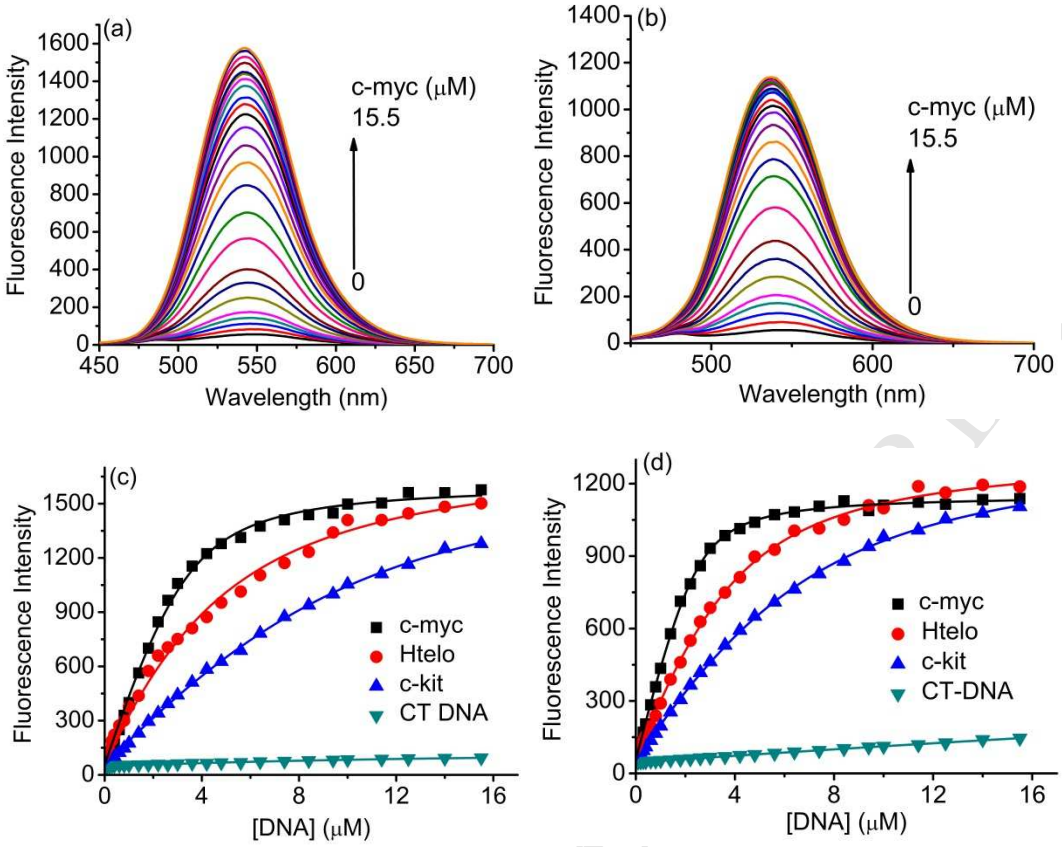

Fig. 2. Fluorescence emission spectra of (a) **3a** (10 μM) and (b) **3b** (10 μM) in HEPES buffer (pH 7.4, 10 mM) containing 0.1 M KCl upon addition of c-myc G-quadruplex (λ_{ex} = 400 nm). Fluorescence intensity of (c) **3a** and (d) **3b** in the presence of various DNA structures determined from fluorimetric titrations. [c-myc] = 0, 0.1, 0.2, 0.3, 0.4, 0.6, 0.8, 1.0, 1.4, 1.8, 2.2, 2.6, 3.0, 3.6, 4.2, 4.8, 5.6, 6.4, 7.4, 8.4, 9.4, 10.0, 11.4, 12.5, 14, 15.5 μM (from bottom to top).

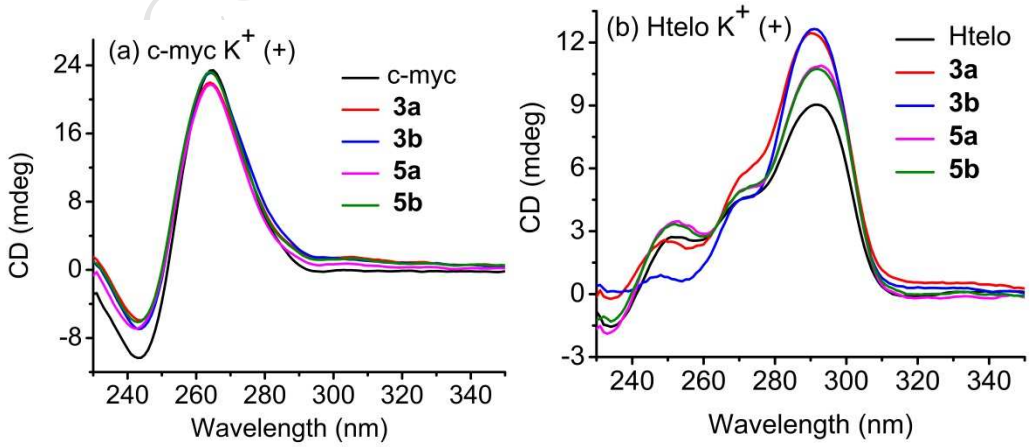

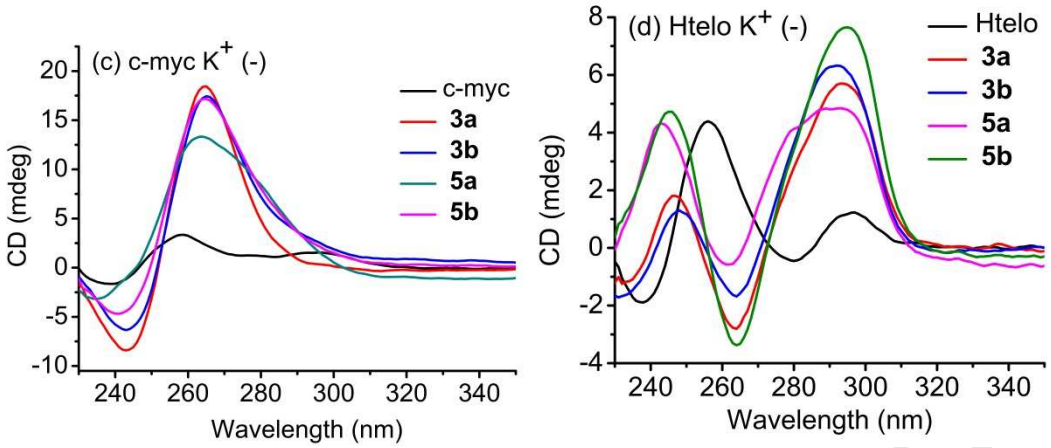

Fig. 3. CD spectra of (a) c-myc and (b) Htelo oligomers upon addition of **3a**, **3b**, **5a** and **5b** in Tris-HCl buffer (pH 7.4, 10 mM) containing 100 mM K^+. CD spectra of (c) c-myc and (d) Htelo oligomers upon addition of **3a**, **3b**, **5a** and **5b** in Tris-HCl buffer (pH 7.4, 10 mM) without K^+. [c-myc] = [Htelo] = 10 μM, [**3a**] = [**3b**] = [**5a**] = [**5b**] = 20 μM.

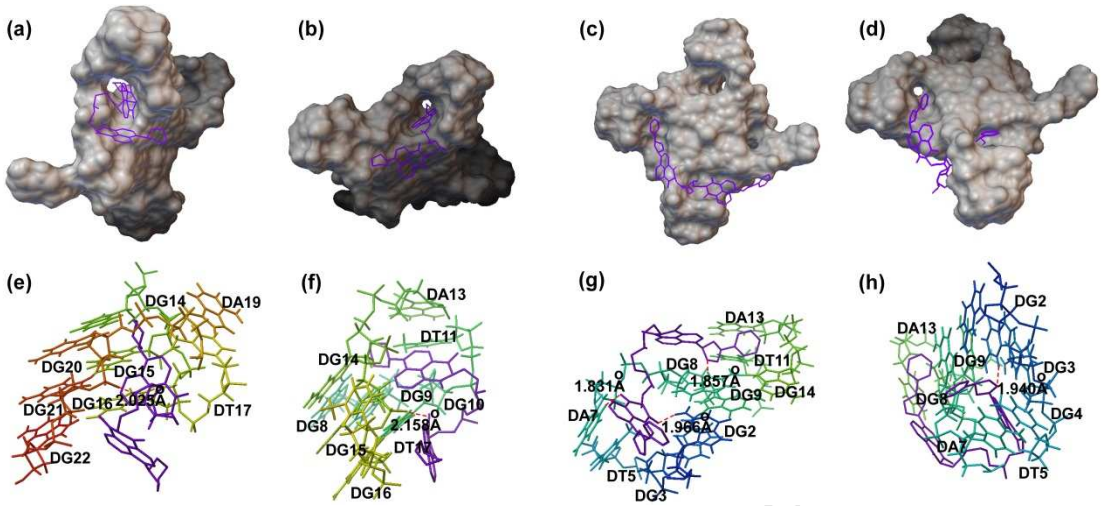

Fig. 4. Overall view of the energy minimized structure for possible binding sites of (a) **3a**, (b) **3b**, (c) **5a** and (d) **5b** with telomeric G-quadruplex (PDB ID: 1KF1). Partial enlargement of molecular models of (e) **3a**, (f) **3b**, (g) **5a** and (h) **5b** with telomeric G-quadruplex. The red dotted line represents the length of the hydrogen bond.

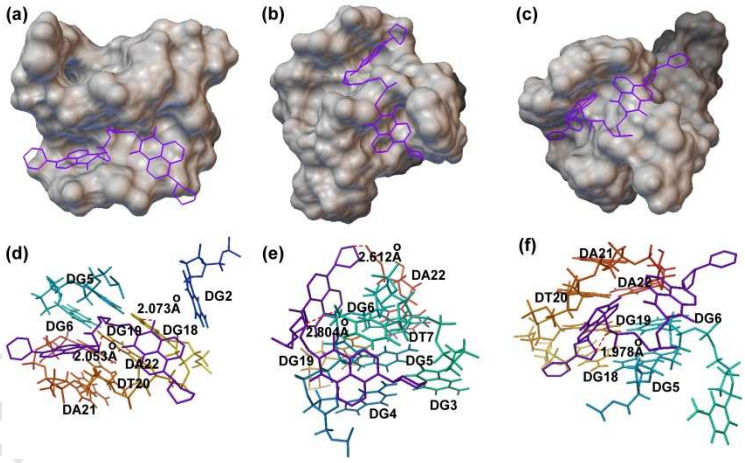

Fig.5. Overall view of the energy minimized structure for possible binding sites of (a) **3a**, (b) **3b** and (c) **5b** with c-myc G-quadruplex (PDB ID: 1XAV). Partial enlargement of molecular models of (d) **3a**, (e) **3b**, and (f) **5b** with c-myc G-quadruplex. The red dotted line represents the length of the hydrogen bond.

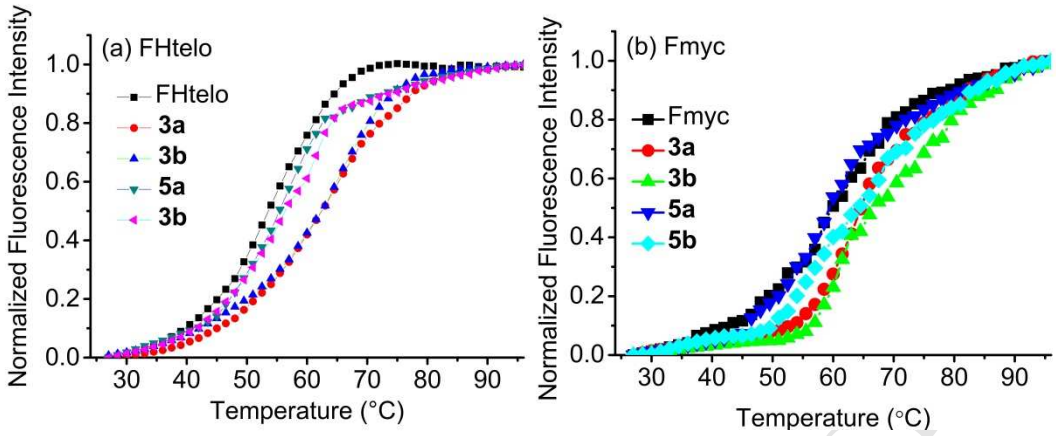

Fig. 6. FRET melting assay of (a) FHtelo and (b) Fmyc with bisnaphthalimide **3a**, **3b**, **5a** and **5b** in 10 mM lithium cacodylate buffer (pH 7.2) containing 10 mM KCl and 90 mM LiCl.

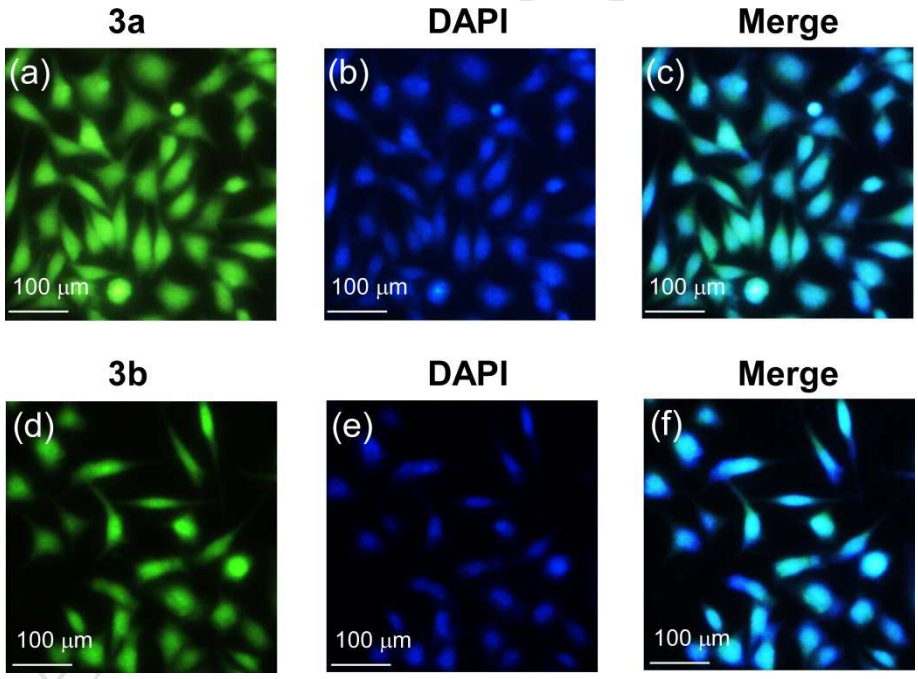

Fig. 7. Double Staining of A549 with (a) **3a** (10 μM), (d) **3b** (10 μM) and DAPI (5 μM) at 37 ℃ for 2 h. Compounds **3a, 3b** and DAPI are excited with a 488 and 405 nm laser, respectively.

High Lights

1. The synthesized bisnaphthalimides possess tumor cell-selective cytotoxic activity.
2. The bisnaphthalimides show high affinity for G-quadruplex (G4) DNA ($K_a > 10^6 M^{-1}$).
3. The bisnaphthalimides can promote the formation and stabilization of G4.
4. A turn-on effect is observed upon interaction of G4 with bisnaphthalimide.